Point Cloud Generation with mmWave MIMO Radar: Measurements and Analysis

L. Felipe Moncada-Calmet ^{1,2,©}, STUDENT, AMTA, Nathan Goodman ^{1,2,©}, MEMBER, AMTA, and Jorge L. Salazar-Cerreño^{1,2,©}, SENIOR, AMTA

(1) The University of Oklahoma, Norman, OK, U.S.

(2) Advanced Radar Research Center (ARRC), Norman, OK, U.S.

Abstract—The MIMO radar technique enables high angular resolution by virtually synthesizing a larger number of receiving antennas [1]. This paper leverages this technique to generate reliable point cloud data of an outdoor space, by applying a series of radar processing techniques and a point cloud denoising function. This work provides a comprehensive explanation of our methodology, from calibration and measurements to data processing and plotting. Our strategy is validated through realworld measurements conducted using the cascaded TI AWR2243 radar, highlighting the potential of mmWave MIMO radars in static 3D mapping scenarios and offering insight into practical implementation challenges.

Index Terms—FMCW, measurements, millimeter wave, MIMO, point cloud generation, radar.

I. INTRODUCTION

With recent advances on the integration of FMCW mmWave radar transceivers, and the improvement of their RF features [2], this technology has become more accessible and therefore more employed in different areas such as Iot, healthcare, environmental and industrial applications and driving assistance systems [3], [4], [5], mainly due to the advantages mmWave frequencies offer in low visibility scenarios, harsh weather conditions, or simply accumulations of mud, dust, or snow [6]. Consequently, it is necessary to provide techniques that keep up with these new technologies.

Several methodologies have been presented in recent years that involve the use of artificial intelligence, such as neural networks [7], [8], [9]. This work presents a simpler and faster strategy for obtaining point cloud data, based on radar signal processing techniques. The focus of this paper is on providing a step-by-step guideline for our measurement procedures and data analysis.

II. SYSTEM DESCRIPTION

Our system (see Figure 1) is divided into five parts: the sensor, the positioner, the stand, the computer, and the scenario. The next subsections explain in detail each of these parts.

A. mmWave Radar

Our sensor is a mmWave evaluation radar designed by Texas Instruments (TI), it features four cascaded AWR2243 radar transceiver chips to achieve fine azimuthal resolution, its specifications are summarized in Table I. This radar allows for two modes of operation, Multiple Input Multiple Output (MIMO) and Beamforming; the entire of this paper is based on the

MIMO mode. This technique improves the angular resolution by virtually increasing the number of receive elements. Extra transmit elements are added in strategic places, so that the phase difference from the received signal keeps its arithmetic progression along the physical receive antennas; in this way, the total number of virtual channels is the number of receive elements multiplied by the number of transmit elements [10]. Each element is a four-patch series-fed antenna array.

TABLE I 4-CHIP AWR2243 RADAR SPECIFICATIONS

Parameters	Value	Unit
Frequencies	77 - 81	GHz
Resolution	1.4 Azimuth	Degrees
FOV	+-70 Azimuth	Degrees
Waveform	FMCW	-
Modes	MIMO / Beamforming	-

B. Robot arm

The positioner is the robot arm UR3e designed by Universal Robots, it features six degrees of freedom and a maximum payload of three kilograms, it comes with a control box and a control panel.

C. Stand and computer

The stand is a caster cart with a bolted aluminum post on the front side, covered with high-frequency absorber foam.

The computer does not appear on the figure, but it is a Lenovo laptop that connects to the radar via an Ethernet cable, it can be seen in Figure 3.

D. Scenario

The scenario is the back patio of the Advanced Radar Research Center (ARRC), Figure 2 shows it. This is an excellent place to demonstrate our algorithm capabilities, as it comprises different structures and materials. On the left there is vegetation, trees, bushes, grass; in the center, a mostly empty space closed by a brick wall, and on the right, some wooden chairs and tables next to a wall with large windows and covered with aluminum sheets.

From this scenario, we will receive different levels of power from different angles. The idea is that our system should be capable of recognizing and discriminating objects, despite the wide variety of shapes and materials in the environment.

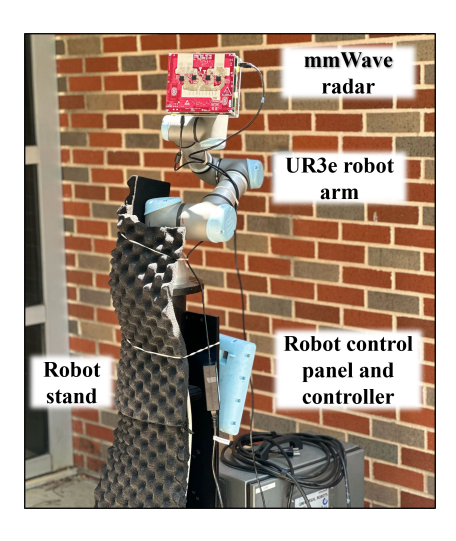


Fig. 1. System setup.

The second thing to consider is that there are no objects moving in this scenario, at least at considerable speeds, that is, because the objective of this paper is to exploit a single chirp information for mapping purposes.

III. DATA COLLECTION

Since the 4-chip AWR2243 radar was designed for automotive applications rather than for mapping of spaces, the high resolution of 1.4 degrees belongs only to the azimuthal dimension. The elevation resolution is 18 degrees, considerably broad for mapping; for this reason, the radar is mounted on the robot arm, so it can accurately tilt it up and down to reliably obtain different layers of data from the space.

For our particular case, we decided to start with a depression angle of 10 degrees and then program the arm to tilt the radar up 5 degrees three times, giving us a total of four measurements at the depression angles of 10, 5, 0, and -5 degrees.

The radar is triggered and controlled from the computer thanks to mmWave Studio software and a customized MAT-LAB app designed to ease the measurement process. Before the measurements, it is important to know that resolution is key for mapping, so the chirp was configured to attain a finer range resolution. Equation (1) presents the range resolution for FMCW radar, where c is the speed of light, and B is the bandwdith of the waveform [11]. So, we maximized our bandwdith and achieved 4.1 cm of range resolution.

$$R_{res} = \frac{c}{2B} \tag{1}$$

These data collected are stored on the MMWCAS-DSP-EVM data capture board, located at the back of the MMWCAS-RF-EVM, the board that holds the RF chips, antennas, and other RF circuitry. These data are later transferred to the computer and processed by our algorithm based on TI's MIMO processing example code.



Fig. 2. Scenario: Back patio at the ARRC.

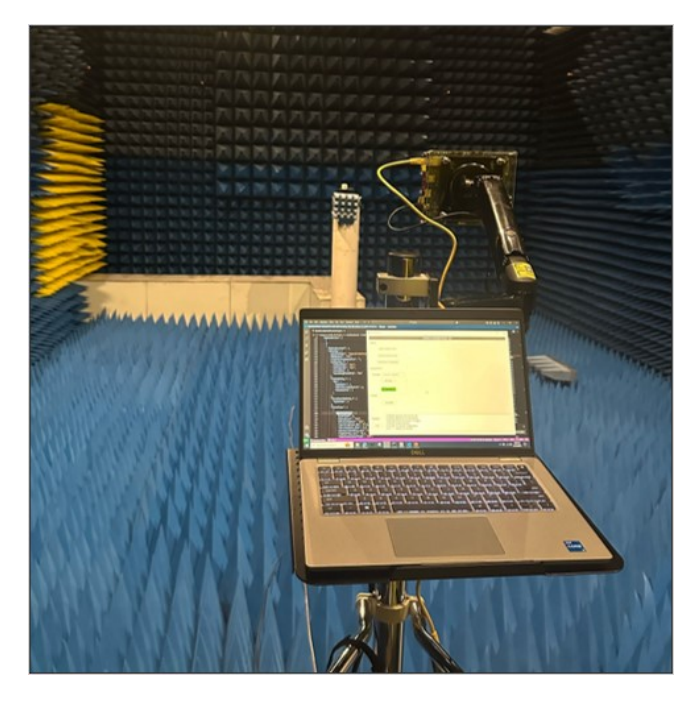


Fig. 3. Radar calibration in an anechoic chamber.

IV. POINT CLOUD GENERATION METHOD

A. Calibration

TI provides a calibration method in which the radar has to be located around 6 meters from a target whose radar cross section (RCS) is approximately $2 m^2$ at 79 GHz.

Therefore, the radar was taken to our largest anechoic chamber. The target and radar were aligned in azimuth and elevation using an industrial self-leveling alignment laser. Then, a measurement was performed and the data obtained were processed with the TI calibration code. This calibration aims to correct for errors in frequency, amplitude, and phase, by providing a set of matrices that can be later applied to our posterior measurements.

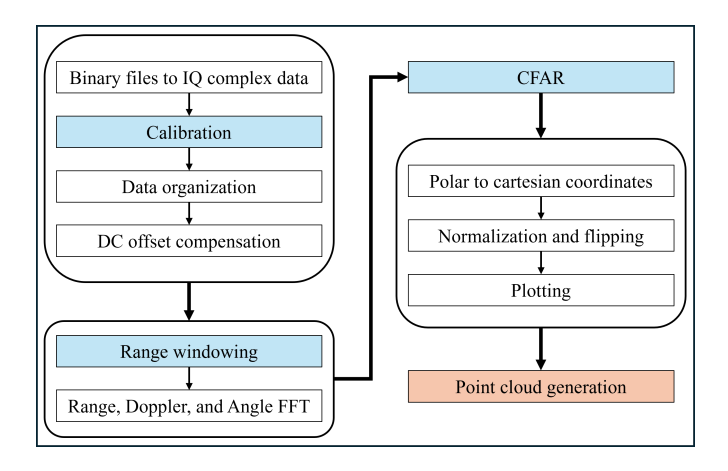


Fig. 4. Data processing flow diagram.

B. MIMO processing

This processing consists of 10 main steps before the point cloud generation, refer to Figure 4. The first step converts the retrieved binary files to IQ complex data, this conversion is very dependent on how the measurement was configured, i.e., the number of chirps sent, the number of samples per chirp, the number of frames, and ultimately the ADC resolution or number of bits of the ADC. The output is then a 4D matrix where the dimensions are, samples per chirp, number of chirps, number of receive elements, and number of transmit elements.

Subsequently, these IQ data were calibrated. In our case, we have only corrected for the phases and amplitudes of our signals. The third step is to organize the data according to the position of the achieved virtual channels. With the AWR2243 TI cascaded radar, 86 non-overlapping virtual channels can be obtained, so the IQ signals have to be correctly organized through these channels. The last step of the data retrieval section is the DC offset compensation; this is done by subtracting from the signals of each virtual channel its mean value.

The next section comprises the heat map or energy map formation steps. First, range windowing is applied to the samples per chirp dimension (usually also called fast-time dimension); the window type applied in our case is Hanning. Windowing is important because it helps to reduce spectral leakage (sidelobes) by decreasing the discontinuities at the edges of our signals [12]. Later in this paper, we will see the effect of this step on the quality of the results. Afterwards, the first FFT (range FFT) is applied along the fast-time dimension, this step focuses the energy of the signals in the range at which they are coming from. This process is also called match filtering. Then, the second FFT would be the Doppler FFT across the chirps (slow-time dimension); a following fftshift should be applied so the 0 Doppler frequency stays in the center of the data. The last FFT should be applied along the virtual channels, followed by a fftshift. The angle FFT focuses the received energy in the directions that correspond to the angles of the incoming signals.

The following section is the detection processing, which is based on a cell averaging constant false alarm rate (CA-CFAR)

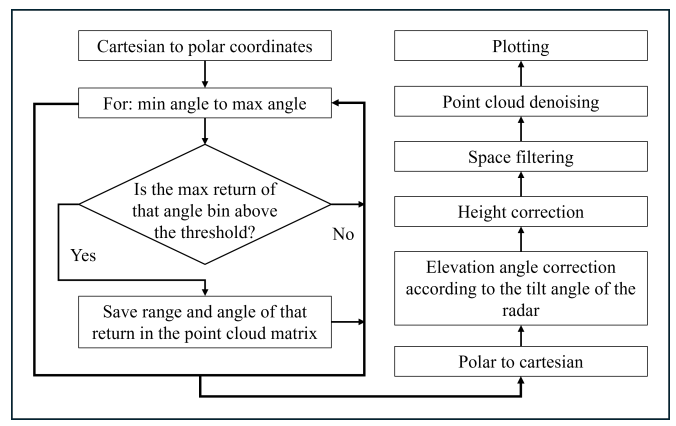


Fig. 5. Point cloud generation diagram.

technique. This is a one-dimensional CFAR applied along the angles, based on the method presented by M. Richards [13].

The subsequent section consists of formatting the data so that it can be plotted and understood correctly by the user. We decided to transform the data from polar to cartesian coordinates, then the energy was normalized, so it can be easily compared with other measurements, flipped or mirrored so it matches our system of coordinates, then the data are converted to a dB scale, and finally plotted.

C. Point cloud generation

Figure 5 presents a flow diagram of the steps performed to obtain a point cloud map of the scene. First, the data are converted back to polar coordinates (the polar coordinates can be taken if they were saved during processing). Then, a "for" loop is used to look for the range of the maximum return for each angle; if the return is above the threshold, the range and angle information are saved in a new x-by-2 matrix. Once all the angles have been scanned, the remaining data are converted to Cartesian coordinates and corrected for the elevation angles corresponding to the tilt angles of the radar for each set of measurements. Then, the height of the radar over the floor should be considered, so an additional correction is applied to account for this offset. Subsequently, since the elevation resolution is considerably coarse, some of the measurement sets, for the lower angles, output points that have negative height, these are clearly errors and should be filtered out; so this is the task of the space filtering block.

So far, all the processing has been performed in MATLAB, mainly because of the expertise and familiarity of the team with this software; however, another important reason is the Add-Ons option that allows to install toolboxes. There is a toolbox called Computer Vision that provides interesting point cloud processing functions such as the "pcdenoise" function, that removes outliers from the point cloud dataset. Although this toolbox was created for LiDAR or camera applications, it also works well for radar too. Finally, for plotting, the MATLAB "scatter3" function is employed.

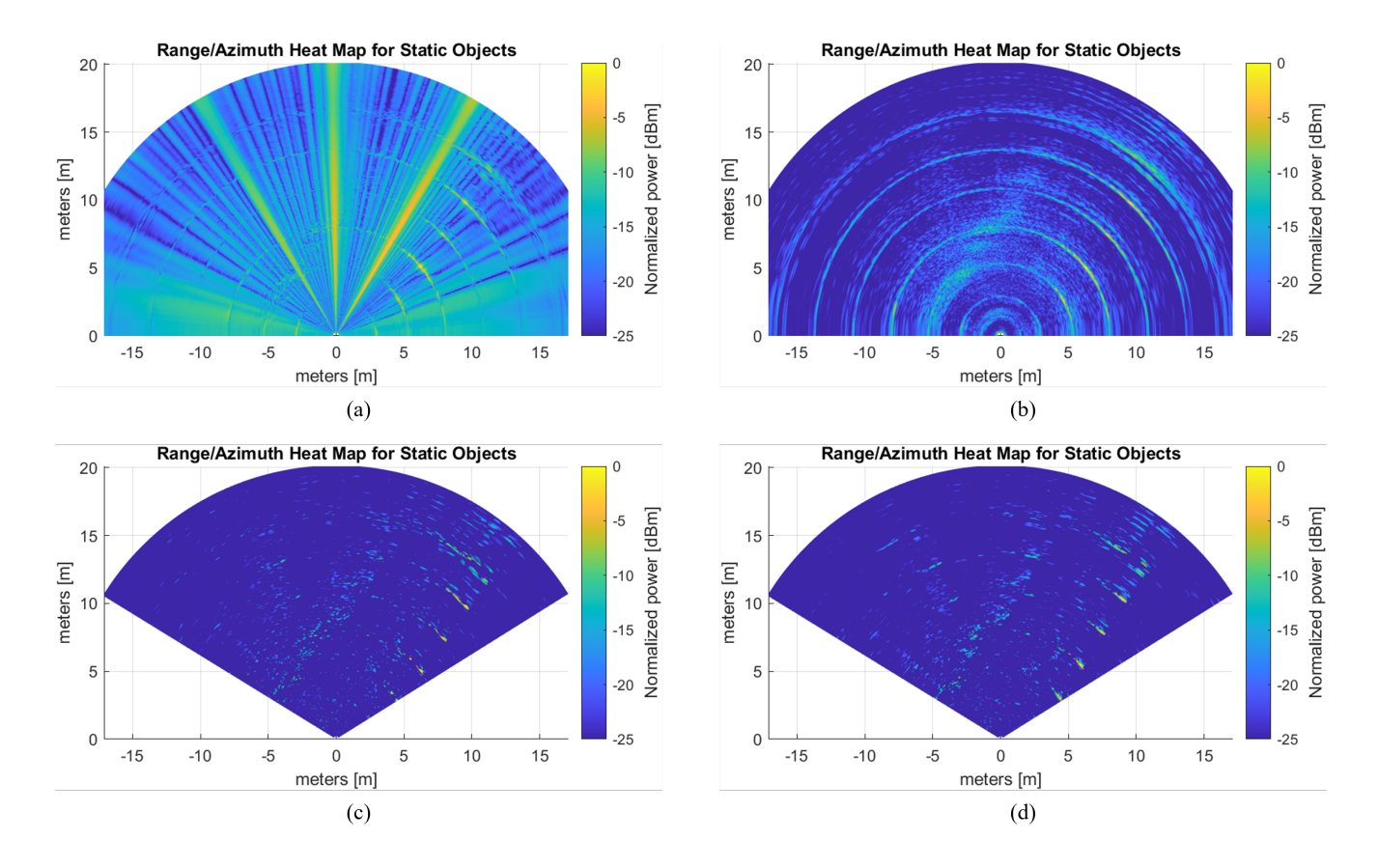


Fig. 6. Data processing sequence. (a) Heat map before range windowing, CFAR and calibration. (b) Heat map after range windowing, but before CFAR and calibration. (c) Heat map after windowing and CFAR, but before calibration. (d) Heat map after range windowing, CFAR and calibration have been applied.

V. ANALYSIS AND RESULTS

Figure 6 illustrates the importance of techniques highlighted in blue light in Figure 4. It is possible to notice the importance of range windowing by looking at the difference between subplot (a) and (b), then the importance of CFAR to get rid of the sidelobes contamination by looking at the improvement in subplot (c), and finally the benefits of calibration are shown in subplot (d), where it is possible to see how the energy spots are more focused and defined. It should be mentioned that the FOV is restricted after the CFAR along angles. The number of angle bins lost on each side is equal to the number of CFAR reference cells, is for this reason that zero padding should be applied during the angle FFT, so we keep as much of our data after CFAR. For this case, we zero padded from 86 elements to 512 elements in the angle dimension.

After processing, in the plot, it is possible to visually recognize several features of our scenario. These features are framed in red in Figure 7. As can be seen, a rectangular-like shape has been formed, it has the same dimensions as our patio, and different elements can be recognized, e.g. the vegetation line, the brick wall at the back, or the downspouts that are highly reflective since they create corner reflectors with the wall. Looking at Figure 2 again, we could see that most of our elements have been captured.

Now, the point cloud generation algorithm is employed

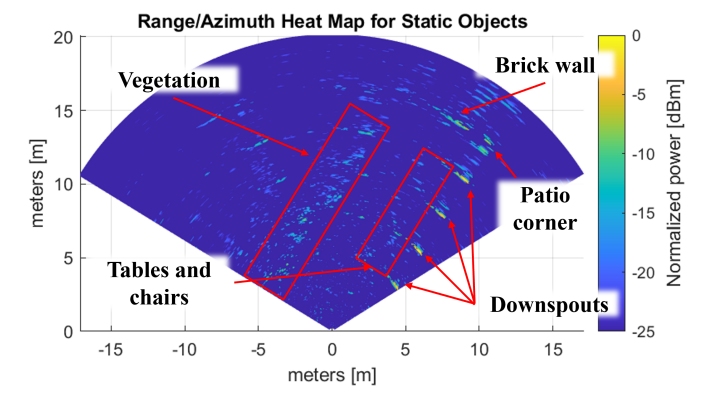


Fig. 7. Visual feature recognition for final heat map.

over the four sets of heat maps. Figures 8 and 9 show an isometric view and a tilted top view of our point cloud output, respectively. From both pictures it is possible to observe four groups of points, the ones that belong to the downspouts on the right side of the plot, the ones that belong to the brick wall at the back of the patio, the ones on the left side that belong to the bushes and trees, and a few points close to the center that could most likely belong to a table or chair. In Figure 9, it is also observable that the different layers of data stack together, and it is also noticeable that there are two

small groups of points outside the patio, the ones on the left beyond the trees, we believe that these correspond to a specific elevated area on the ground, since the backyard goes uphill. Regarding the points beyond the brick wall, we have to say that unfortunately these are errors and most probably exist due to multipath reflections.

In terms of the sparsity of this point cloud, we should mention that, in comparison with LiDAR or camera, radar point clouds are very sparse due to the poor resolution [7]; nonetheless, despite all the techniques applied, that reduce the number of points, to improve the detection of elements in our scenario, e.g. CFAR and denoisoing, the surface limits of the surrounding were decently defined in an open large space.

It is important and necessary to mention that, for the sake of providing a replicable methodology, the aforementioned threshold for the point cloud generation was determined as -15 dB below the maximum return; and the CFAR parameters as reference and guard cells and K factor were calculated ad hoc.

Finally, in a manner of discussion, it was seen that if CFAR is applied along range, more characteristics of the scene are retrieved; however, the sidelobe contamination persists; in this case, if algorithms such as Nulling or CLEAN are performed to remove the strong reflective points (downspouts), more information could have been retrieved, and the point cloud could have been generated by parts; however, these procedures extend beyond the scope but could be analyzed in a future paper.

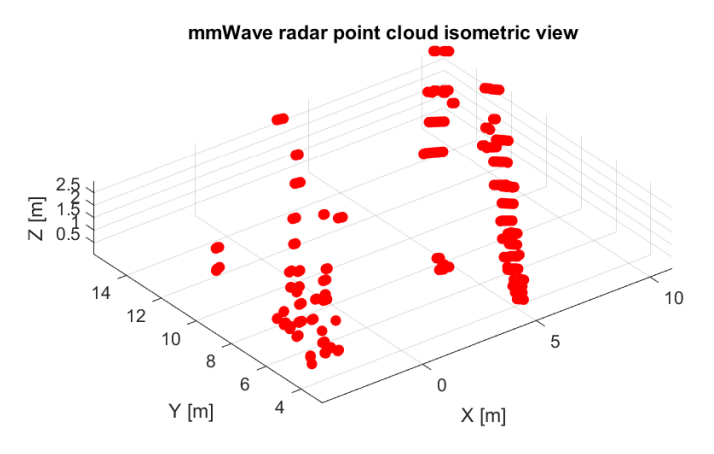


Fig. 8. Point cloud - Isometric view.

VI. CONCLUSION

It is viable to obtain reliable point cloud data from a diverse scenario with a mmWave MIMO radar. The algorithm presented is fast, since only processes a single chirp, and does not depend on artificial intelligent techniques. This algorithm is also easy to implement, being the most complicated operations the FFTs and the denoising function, which is based on statistical techniques [14].

ACKNOWLEDGEMENT

This work is supported by the Advanced Radar Research Center (ARRC) at The University of Oklahoma.

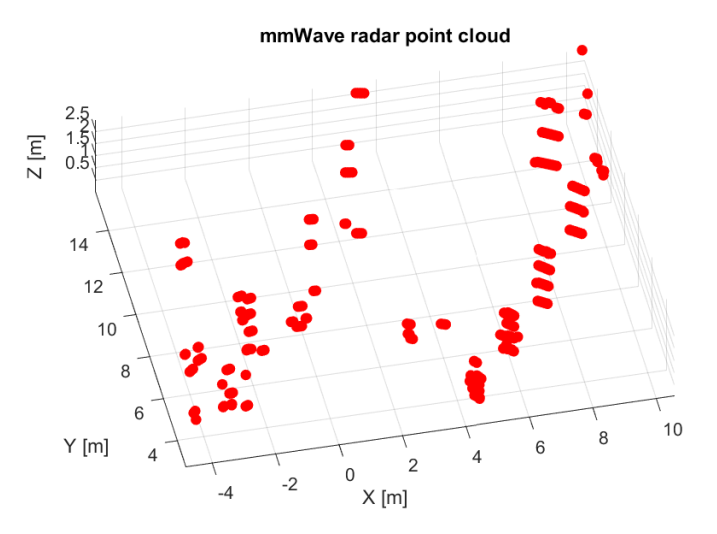


Fig. 9. Point cloud - top tilted view.

REFERENCES

- [1] Y. Kalkan, "20 years of mimo radar," *IEEE Aerospace and Electronic Systems Magazine*, vol. 39, no. 3, pp. 28–35, 2024.
- [2] F. Schwartau, S. Preussler, M. Krueckemeier, F. Pfeiffer, H. Stuelzebach, T. Schneider, and J. Schoebel, "Modular wideband high angular resolution 79 ghz radar system," in 2019 12th German Microwave Conference (GeMiC), 2019, pp. 194–197.
- [3] H. D. Mafukidze, A. K. Mishra, J. Pidanic, and S. W. P. Francois, "Scattering centers to point clouds: A review of mmwave radars for non-radar-engineers," *IEEE Access*, vol. 10, pp. 110 992–111 021, 2022.
- [4] J. Chen, W.-H. HUNG, and K.-L. WU, "Estimation of water surface velocity using fmcw radar with on-chip antenna," in 2024 IEEE Asia-Pacific Microwave Conference (APMC), 2024, pp. 940–942.
- [5] M. Khan, R. Shamim, M. Wajid, and A. Srivastava, "Optimized hard-ware architecture for respiration rate classification using quadratic svm and mmwave radar sensor," in 2025 IEEE International Symposium on Circuits and Systems (ISCAS), 2025, pp. 1–5.
- [6] W. Jones, "Keeping cars from crashing," *IEEE Spectrum*, vol. 38, no. 9, pp. 40–45, 2001.
- [7] Y. Cheng, J. Su, M. Jiang, and Y. Liu, "A novel radar point cloud generation method for robot environment perception," *IEEE Transactions on Robotics*, vol. 38, no. 6, pp. 3754–3773, 2022.
- [8] B. Tan, Z. Ma, X. Zhu, S. Li, L. Zheng, S. Chen, L. Huang, and J. Bai, "3-d object detection for multiframe 4-d automotive millimeter-wave radar point cloud," *IEEE Sensors Journal*, vol. 23, no. 11, pp. 11125– 11138, 2023.
- [9] O. Schumann, M. Hahn, J. Dickmann, and C. Wöhler, "Semantic segmentation on radar point clouds," in 2018 21st International Conference on Information Fusion (FUSION), 2018, pp. 2179–2186.
- [10] D. Bliss and K. Forsythe, "Multiple-input multiple-output (mimo) radar and imaging: degrees of freedom and resolution," in *The Thrity-Seventh Asilomar Conference on Signals, Systems & Computers*, 2003, vol. 1, 2003, pp. 54–59 Vol.1.
- [11] M. Song, J. Lim, and D.-J. Shin, "The velocity and range detection using the 2d-fft scheme for automotive radars," in 2014 4th IEEE International Conference on Network Infrastructure and Digital Content, 2014, pp. 507–510.
- [12] A. Oppenheim and R. Schafer, Discrete-Time Signal Processing. Pearson Deutschland, 2013. [Online]. Available: https://elibrary.pearson. de/book/99.150005/9781292038155
- [13] M. Richards, Fundamentals of Radar Signal Processing, ser. Professional Engineering. McGraw-Hill Education, 2005. [Online]. Available: https://books.google.com/books?id=j91oJ22ldoQC
- [14] R. B. Rusu, N. Blodow, Z. Marton, A. Soos, and M. Beetz, "Towards 3d object maps for autonomous household robots," in 2007 IEEE/RSJ International Conference on Intelligent Robots and Systems, 2007, pp. 3191–3198.